

# DESY SUMMER STUDENT REPORT

---



## Characterization of Fe-based nanoparticles by X-ray Diffraction

**Bc. Petra Hajdová**

TUKE, Slovakia

*(September 5, 2013)*

*Supervisor*

RNDr. Jozef Bednarčík, PhD.

Deutsches Elektronen Synchrotron DESY

Notkestrasse 85

22607 Hamburg, Germany

# Abstract

The subject of this thesis is the study of spherical nanoparticles on iron base prepared by control precipitation in Cu-Fe alloy. The phase composition of these nanoparticles was evaluated from the X-ray diffraction measurements and the local atomic structure was characterised using Pair Distribution Function (PDF).



# Contents

|          |  |          |
|----------|--|----------|
| <b>1</b> | <b>Introduction.....</b>                       | <b>1</b> |
| <b>2</b> | <b>Goals of the research project .....</b>     | <b>1</b> |
| <b>3</b> | <b>Sample preparation.....</b>                 | <b>2</b> |
| <b>4</b> | <b>Pair distribution functions (PDF) .....</b> | <b>4</b> |
| <b>5</b> | <b>P02.1 beamline at PETRA III, DESY.....</b>  | <b>5</b> |
| <b>6</b> | <b>Result and Discussion .....</b>             | <b>5</b> |
|          | <b>References.....</b>                         | <b>8</b> |

---

## 1 Introduction

Nanoparticles (NPs) are simply particles in the nanosize range ( $10^{-9}$  m), usually <100 nm in size. In the narrower sense, they are regarded as the particles smaller than 10-20 nm, where the physical properties of solid materials themselves would drastically change. The main reason for having new physical properties, unseen in either smaller or bigger objects, is a higher ratio of atoms on the surface of the object in relation to the total amount of atoms, and a growing influence of quantum effects that strongly manifest themselves on electrical, magnetic and optical properties.

Magnetic properties of nanometer scale particles are promising for various important technological applications. When the size of ferromagnetic particles tends towards some nanometres, they become a single domain exhibiting a number of unique physical properties. Magnetic nanoparticles (MNPs) have many unique magnetic properties such as superparamagnetism, low Curie temperature, high coercivity, high magnetic susceptibility, etc. [1-2].

Iron oxide is the material that is investigated the most in biomedical techniques, due to its superior biocompatibility with respect to other magnetic materials. Iron oxide nanoparticles have recently attracted much attention due to their virtues of low toxicity, biocompatibility and environmental friendliness. They can be used as magnetic resonance imaging agents in diagnostic, heat mediators in hyperthermia treatments, hyperthermia treatment of cancer and as magnetic guidance in drug delivery applications.

In the last years, several new methods of nanoparticle synthesis have been developed, which satisfy the quantitative and qualitative demands on various levels. For nanoparticles to be applicable practically, like in targeted transport of medication or curing of cysts through local hyperthermia, they need to be precisely characterised [1-2].

## 2 Goals of the research project

Goals of this project can be divided into two main parts:

- experimental determination of pair distribution functions (PDF),
- study of local atomic structure of selected nanomaterials.

---

### 3 Sample preparation

Studied iron-based nanoparticles were prepared at Department of Materials Science, Faculty of Metallurgy at Technical University of Košice by combination of thermally induced precipitation from the Cu-Fe solid solution followed by chemical extraction of the particles from the matrix [3].

The Cu-Fe alloy with a low Fe content is precipitally hardenable thanks to the drop in the dissolvability of iron in copper, while the maximum saturation of the solid solution at a temperature of 1084 °C is 4.1% Fe and as the temperature declines, the dissolvability declines down to a value of zero upon reaching the temperature of its surroundings.

The process of creating the basic feedstock for the creation of nanoparticles is discussed in Ing. Ondrej Milkovič, PhD.'s dissertation. Samples cut from the raw pipe material were subject to thermal processing, which consisted of dissolvable and precipitative annealing, that ensured the manufacture of precipitates with controlled size and morphology.

While thermally processing, the Cu-Fe alloy gets annealed at the temperature of dissolutive annealing and then gets stabilised by rapid cooling, which ensures that the material enters its default state. Samples of oversaturated solid solution have been subjected to precipitative annealing at three different temperatures with various durations of annealing (see tab. 1). The last phase is the chemical dissolution of the copper matrix, as the solution with Fe-nanoparticles emerges. After being rinsed and dried, the final product is in the form of a powder [4].

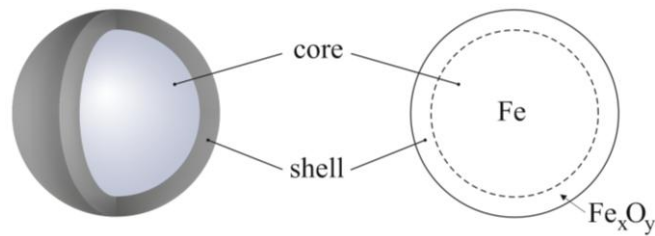
In tab. 1, you can see the samples' codes, temperature, and time of precipitative annealing. Only those samples, which have been highlighted in color, have been analysed.

---

**Tab. 1 Temperature and annealing time for different samples**

| Sample | Temperature<br>[°C] | Annealing time<br>[hour] |
|--------|---------------------|--------------------------|
| A      | 700                 | 3                        |
| B      |                     | 6                        |
| C      |                     | 9                        |
| D      |                     | 12                       |
| E      |                     | 18                       |
| F      | 600                 | 3                        |
| G      |                     | 6                        |
| H      |                     | 9                        |
| I      |                     | 12                       |
| J      |                     | 18                       |
| K      | 500                 | 3                        |
| L      |                     | 6                        |
| M      |                     | 9                        |
| N      |                     | 12                       |
| O      |                     | 18                       |

Based on previous measurements, the prepared nanoparticles have a core-shell structure. On the fig. 1, you can see a schematic drawing of a core-shell-type structured nanoparticle, which is typical for an iron nanoparticle, due to its high level of pyrophoricity [4].

**Fig. 1 Core-shell structured nanoparticles (modified by [4])**

In most case pyrophoricity causes nanoparticles to have a different surface structure and core structure. While the core consists of an  $\alpha$ -Fe phase, the surface is

---

passivised by a growing oxidic layer ( $\alpha$ -Fe<sub>2</sub>O<sub>3</sub>,  $\gamma$ -Fe<sub>2</sub>O<sub>3</sub>, Fe<sub>3</sub>O<sub>4</sub>, FeOOH and etc.), based on the conditions of production [1].

## 4 Pair distribution functions (PDF)

The PDF gives the probability of finding an atom at a given distance  $r$  from another atom. In other words it can be understood as a bond length distribution (fig. 2).

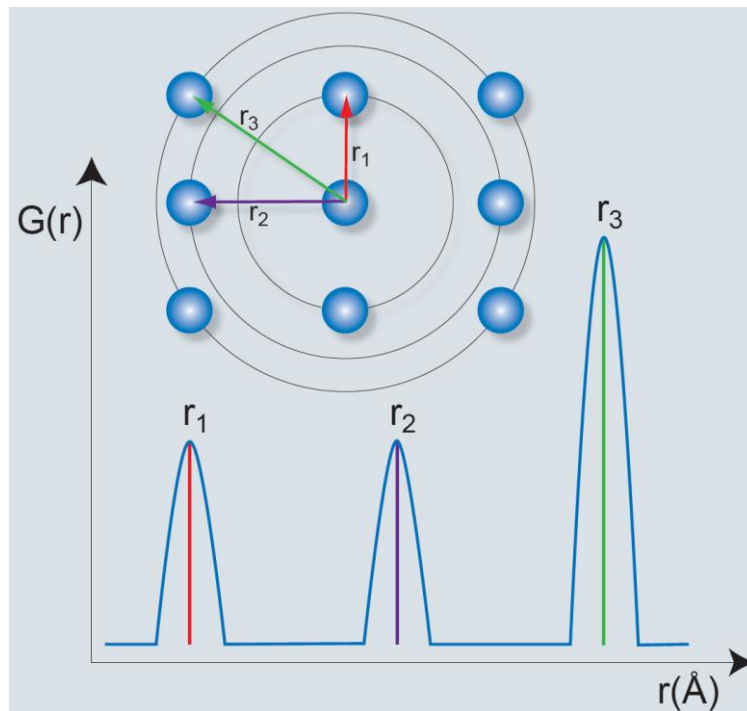


**Fig. 2 Principle of the PDF. Inter-atomic distances  $r_i$  cause maxima in the PDF  $G(r)$ . The area below the peaks correspond to the coordination number [5]**

In this project X-ray diffraction data has been corrected for:

- background (air) scattering,
- inelastig (Compton) scattering,
- multiple scattering,
- fluorescence,
- absorption correction,
- Laue diffuse scattering.

Performing of all corrections and calculation of structure factor and pair distribution function was performed with help of PDFgetX2 program [6].

---

## 5 P02.1 beamline at PETRA III, DESY

The measurements were performed at the P02.1 beamline, which operates with fixed photon energy of 60 keV ( $\lambda = 0.20727 \text{ \AA}$ ). LaB<sub>6</sub> standart was used to calibrate the sample-to-detector distance. Experimental setup is schematically drawn in fig. 3.

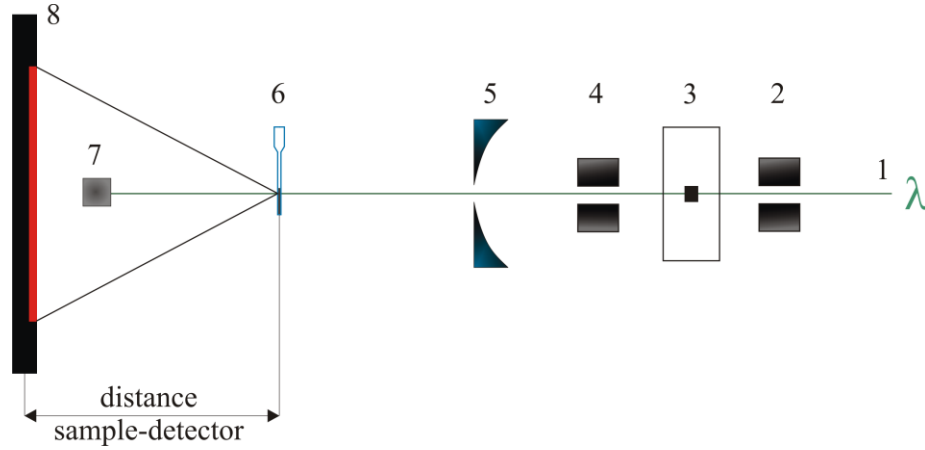
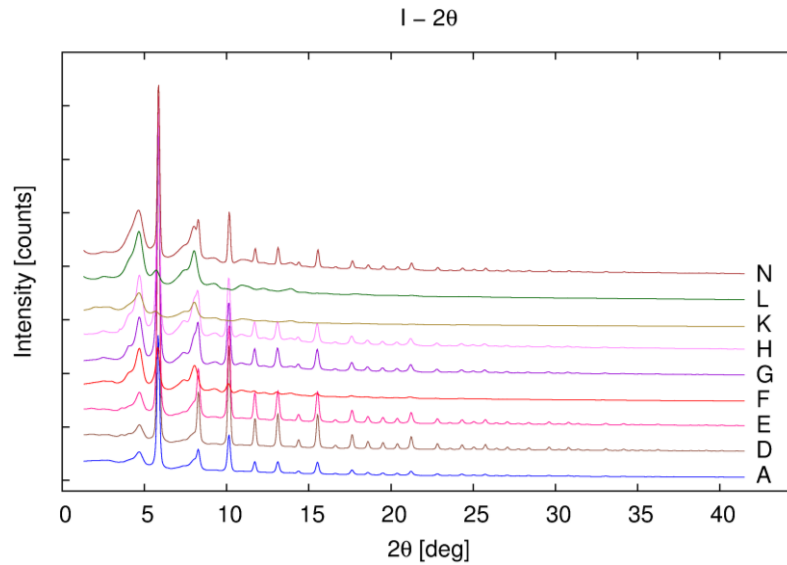


**Fig. 3** Schematic drawing of the experimental setup: (1) X-ray beam, (2) primary slits, (3) small shutter, (4) secondary slits, (5) pinhole, (6) sample in capillary, (7) beam stop, (8) detector Perkin Elmer 1621 (2048×2048 pixels, pixel size 0.2×0.2 mm<sup>2</sup>)

## 6 Result and Discussion

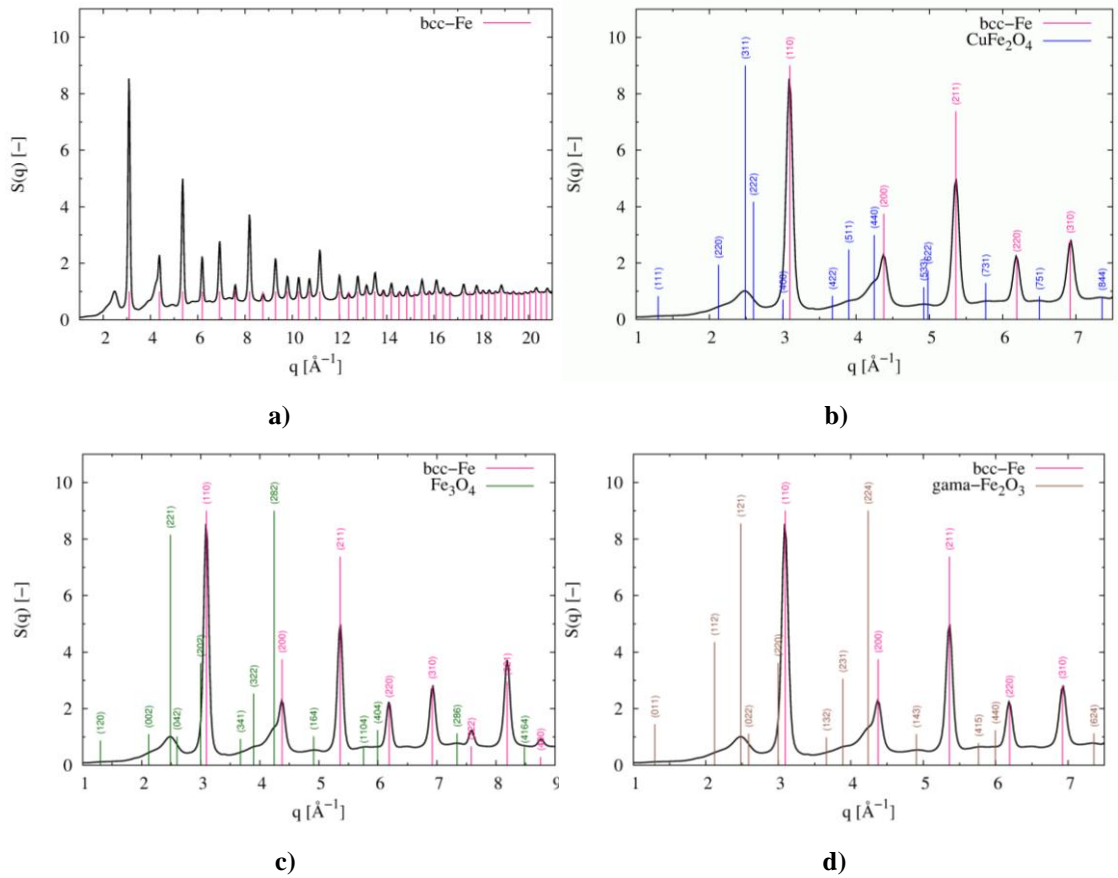
Two dimensional X-ray diffraction patterns were reduced to one dimensional intensity distribution using FIT2D [7]. This procedure is called radial integration.

Fig. 4 shows the diffractions of all the analysed samples after radial integration.



**Fig. 4** X-ray diffraction of all analyzed samples

Phase analysis was asserted using a PCW program [8], the phases used were ones from Inorganic Crystal Structure Database (ICSD). As can be seen on fig. 5a, the major phase is  $\alpha$ -Fe, with higher peaks. After zooming in, new peaks, which don't belong to  $\alpha$ -Fe, become visible. There's at least one minor phase present in the nanoparticles. Candidates for the minor phase are:  $\text{CuFe}_2\text{O}_4$  (fig. 5b),  $\text{Fe}_3\text{O}_4$  phase (fig. 5c) and  $\gamma\text{-Fe}_2\text{O}_3$  phase (fig. 5d). The peaks of major phase are narrow, while the minor phase reveals much wider peak. This suggest that the minor phase exhibits higher degree of structural disorder.



**Fig. 5 Structure factor of sample A**

- a) vertical pink lines depict peaks position of bcc-Fe phase**
- b) vertical blue lines depict peaks position of  $\text{CuFe}_2\text{O}_4$  phase**
- c) vertical green lines depict peaks position of  $\text{Fe}_3\text{O}_4$  phase**
- d) vertical brown lines depict peaks position of  $\gamma\text{-Fe}_2\text{O}_3$  phase**

Due to the difficulty of assessing the chemical composition of nanoparticles, the results are based on an estimation of: 90% Fe, 8%  $\text{O}_2$ , 2% Cu [at. %]. Changing the ratios of the elements did not constitute a change in the character of oscillations



appearing of PDF – only their amplitudes are changed. Figure 6a shows PDF function of the sample A. Oscillations vanish at the value of  $r \sim 75 \text{ \AA}$ , which corresponds to the mean value of the particles size. Figure 6b shows part of the PDF function of the sample A together with the PDF function of  $\alpha$ -Fe, that has been calculated in PDF GUI [6]. Most of the peaks match up, confirming that the nanoparticles are made up mostly of  $\alpha$ -Fe. Peaks denoted with a arrow correspond to the minor phase. The PDF functions of samples A, D and E (precipitative temperature of  $700 \text{ }^\circ\text{C}$ ) are shown in fig. 6c. It is seen that the phase-composition of these nanoparticles does not change with the duration of precipitative annealing.

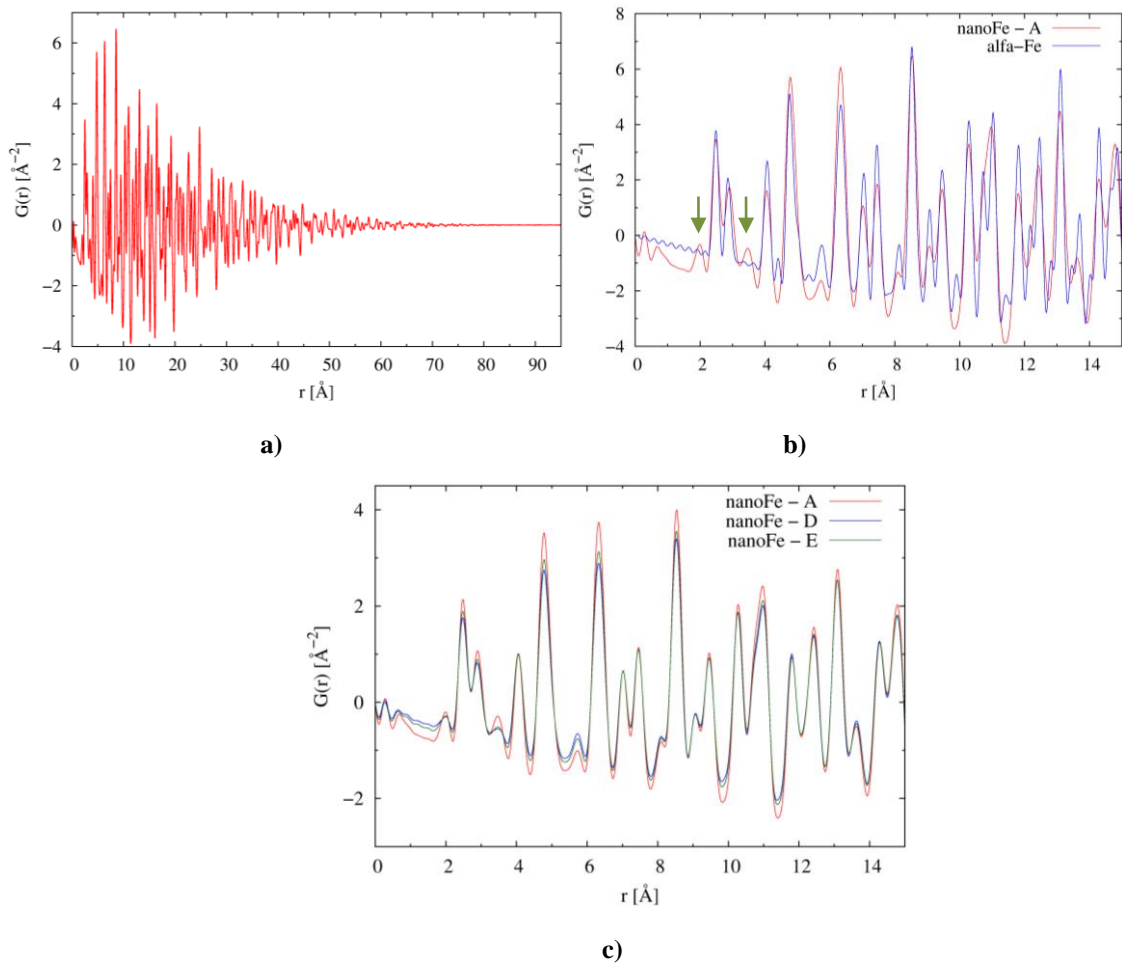


**Fig. 6 Pair distribution functions**

**a) of sample A**

**b) of sample A and  $\alpha$ -Fe (detailed view)**

**c) of samples A, D and E (detailed view)**

All presented data are preliminary and full evaluation of the analysed samples will be presented in my diploma thesis.

---

## References

- [1] GUPTA, A. K. – GUPTA, M.: *Synthesis and surface engineering of iron oxide nanoparticles for biomedical applications*. In: Biomaterials, Volume 26, Issue 18, June 2005, Pages 3995-4021
- [2] C. N. RAO – A. MÜLLER – K. CHEETHAM: *The Chemistry of Nanomaterials: Synthesis, Properties and Applications*, 2005. ISBN: 9783527306862
- [3] Ondrej MILKOVIČ – Štefan NIŽNÍK – Svätoboj LONGAUER: *Isolating Fe-nanoparticles using chemical separation*. Patent application: 104-2010, registered 22. 09. 2010
- [4] Ondrej MILKOVIČ: *Production of Fe-based nanoparticles*. PhD thesis. Košice: Technical University of Košice, Faculty Of Metallurgy, 2007, 117 p.
- [5] K. KNORR – B. HINRICHSSEN – Bruker AXS: *Determination of Pair Distribution Functions (PDF)* [online] <[http://www.bruker.com/fileadmin/user\\_upload/8-PDF-Docs/X-rayDiffraction\\_ElementalAnalysis/XRD/Flyers/Determination\\_of\\_PDF\\_Flyer\\_DOC-H88-EXS031.pdf](http://www.bruker.com/fileadmin/user_upload/8-PDF-Docs/X-rayDiffraction_ElementalAnalysis/XRD/Flyers/Determination_of_PDF_Flyer_DOC-H88-EXS031.pdf)>
- [6] X. QIU – J. W. THOMPSON – S. J. L. BILLINGE: *PDFgetX2: a GUI-driven program to obtain the pair distribution function from X-ray powder diffraction data*. In: J. Appl. Crystal. 2004, 37, 678-678
- [7] A. P. HAMMERSLEY – S. O. SVENSSON – M. HANFLAND – A. N. FITCH – D. HÄUSERMANN: *Two-Dimensional Detector Software: From Real Detector to Idealized Image or Two-Theta Scan*. In: High Pressure Research, Volume 14, 1996, pp. 235-248.
- [8] W. KRAUS – G. NOLZEB: *POWDER CELL – a program for the representation and manipulation of crystal structures and calculation of the resulting X-ray powder patterns*. In: Journal of Applied Crystallography, Volume 29, Part 3, 1996, pp. 301-303. DOI: 10.1107/S0021889895014920